Supplementary Material Table of Contents

Table S1. Oligonucleotides and primers used in this study.

Plasmid/siRNA	*OCRL* exon target	Sequence (5'-3')
pX330	13	F: AAACCGAATTTCAAGAGTCTCTGAT
		R: TAAAATCAGAGACTCTTGAAATTCG
pHRS	13	F: AATTATGCTTAAAGTTCTCAGAGACTTCCG
		R: GATCCGGAAGTCTCTGAGAACTTTAAGCAT
PCR	13	F: TCCTTAGGGTTGTCATTTGGTT
		R: TAAGACGTTTCCATCACTCCCT
siRNA construct 1	17	GGTTCCCTGCCATTTTTCA
siRNA construct 2	15/16	GGGUGAAGGUUGUGGAUGUUU

Table S2. Potential off-targets of CRISPR/Cas9 *OCRL* guide sequence.

Gene	Protein	% Match	Chrom. Loc.	Function	Expressed in Kidney
TMEM117 (isoform X3)	Transmembrane protein 117	82.6	12	Unknown	Low - Moderate
ARHGAP17 (isoform X3)	Rho-GTPase-activating protein 17	65.2	16	Involved in tight junction maintance by regulating activity of CDC42. GTPase activator	Moderate
LCMT1 (isoform a)	Leucine carboxyl methyltransferase 1	65.2	16	Methylates carpoxyl group of the C-terminal leucine residue of protein phosphatase 2A catalytic subunits	Moderate - High
ZNF717	Zinc finger protein 717-like	60.9	22	May be a transcription factor	Yes
OR11H1	Olfactory receptor 11H1	60.9	22	Odorant receptor	None

No off-target events were reported on CHOPCHOP during guide selection. The guide sequence was blasted against the GRCh38.p2. edition of the human genome for a more conservative analysis of off-target effects. Top hits that contained the required PAM sequence are listed. UniProt and Expression Atlas were used to interpret protein function and expression. As none of the top hits match 100% to the guide and few have importance to our system, off-target effects are considered to be unlikely.

Supplementary Figure Legends

Figure S1. CRISPR/Cas9 *OCRL* clones have no OCRL expression. CRISPR/Cas9 *OCRL* knockout clone lysates were western blotted to detect OCRL and β-actin. No expression of either truncated or full length OCRL was evident.

Figure S2. OCRL depletion slows proliferation of HK-2 cells without increasing apoptosis. Equal numbers (400,000 cells) of CRISPR/Cas9 control cl.1, KO cl.1, or KO cl.2 cells (A,B) or HK2 cells transfected with control or *OCRL* siRNA (C,D) were plated on Transwell filters, and cultured for four days, fixed, and stained with DAPI to visualize nuclei. Random fields were acquired and representative images are shown in (A and C). Nuclei were quantitated using the MatLab program described in Long et al. (2017) *Mol. Biol. Cell* 28:2508-2517. Nuclei/field (mean and individual points; five fields per condition in two or three independent experiments) is plotted in (B and D). (E) CRISPR/Cas9 Control cl.1, KO cl.1 and KO cl.2 were incubated with Biotium NucView 488 Caspase-3 substrate and imaged live every 20 min for 4.7-11.3 h. Cells undergoing apoptosis were identified by an increase in fluorescence signal and the percentage of apoptotic cells in each condition is plotted [mean and individual points of five independent experiments (four with KO cl.2 and one with KO cl.1)]. (F) Knockdown efficiency in HK-2 cells transfected with control or *OCRL* siRNA was confirmed by western blotting lysates with anti-OCRL antibodies and normalized to β-actin. OCRL depletion ranged from 70-95% and was depleted by 92% in the representative experiment shown. Scale bar (A and C): 10 μm. *p<0.05 by one-way ANOVA, Dunnett's multiple comparisons test in (B).

Figure S3. *OCRL* knockdown increases multinucleation in mRPTC and hRPTC cell lines. Mouse (mRPTC, A-C) and human (hRPTC, D-F) renal proximal tubule cells were transfected with control or *OCRL* siRNA. Knockdown efficiency was quantified by western blotting and was typically 40-50% for mRPTCs (43% in the experiment shown in A) and 90-97% in hRPTCs (97% in the experiment shown in D). (B and E) Wheat germ agglutinin and DAPI were used to visualize cell borders and nuclei, respectively. Representative images of control siRNA mononuclear cells in samples transfected with control siRNA and multinucleated cells in samples treated with *OCRL* siRNA are shown. (C and F) The percentage (mean and individual points) of cells with multiple nuclei is plotted (panel C, three independent experiments; 261-539 cells per condition scored in each experiment; panel F, two independent experiments; 114-295 cells per condition scored in each experiment). Scale bar (B and E): 10 μm. * p<0.05 and *** p<0.001 based on unpaired t test in (C) and (F).

Figure S4. Effect of reduced V_{max} on PT uptake of albumin and LMWP. (A) Albumin/creatinine ratio and (B) LMWP/creatinine ratio models with reductions in V_{max}. Each line corresponds to a model solution using a V_{max} that is 100-50% of the fit value. A 33% and 32% reduction in V_{max} in the absence of proximal tubule shortening is predicted to result in a similar urinary excretion profile of albumin and LMWP, respectively, similar to that observed in LS, although it cannot explain the additional PT dysfunction in the disease. Changes in V_{max} could also be relevant to tubular proteinuria in other genetic diseases, such as Dent disease. The effect of varying V_{max} on urinary protein excretion of albumin (C) and LMWP (D) when SNGFR is reduced by 20% is plotted. Under this condition, a 41% and 43% reduction in V_{max} would produce the predicted urinary excretion profiles of albumin and LMWP, respectively. In each graph, the black arrow denotes the expected urinary protein excretion ratio (mg/mmol creatinine) at the distal end of the PT of LS patients.

Figure S5. *Ocrl* morphant zebrafish injected with *ocrl* morpholino have shorter pronephric kidney segments. *In situ* hybridization of megalin/*lrp2a*, a proximal tubule marker, and *cdh17*, a pronephric tubule marker, was performed in uninjected controls and in zebrafish injected with 6ng or 8 ng of *ocrl* morpholino (MO) at 72 hpf. The distributions of *lrp2a* (A) and *cdh17* (C) expression in representative zebrafish are shown. Scatter plots show the length of *lrp2a* (B) and *cdh17* (D) positive segments (mean +/- SD; *lrp2a*, n=22-38; *cdh17*, n=48-80). (E) Ratio of average *lrp2a* length over average *cdh17* length was compared across conditions. ** p<0.01 *** p<0.001 **** p<0.0001 based on one-way ANOVA via Tukey's multiple comparisons test in (B) and (D).

Figure S6. Acute or chronic depletion of OCRL does not impair endocytic uptake in HK-2 cells. Control or *OCRL* knockout clones (A and B) or cells transfected with control or *OCRL* siRNA (C and D) were incubated under static conditions or exposed to orbital fluid shear stress (FSS) for 1 h in the presence of Alexa Fluor 647-albumin, then fixed, imaged, and albumin uptake quantified as described in Methods. Representative fields are shown in (A) and (C). (B) Albumin uptake was normalized to that under static conditions in each clone, and the fold change (mean +/- SE) of three independent experiments is plotted. (D) Data were normalized to uptake under static conditions and the mean fold change +/- SE of three independent experiments is plotted. Scale bars (A and C): 25 μm. * $p<0.05$ ** $p<0.001$ *** $p<0.005$ based on a two-way ANOVA via Sidak's multiple comparisons test in (B).

Figure S7. Cilia length in siRNA treated and CRISPR/Cas9 *OCRL* knockout clones. HK-2 cells treated with either control or *OCRL* siRNA (A, B) or CRISPR/Cas9 control and *OCRL* KO clones (C, D) were fixed and processed for immunofluorescence to visualize acetylated tubulin and nuclei. Representative images of cells with cilia of approximately median length for each condition are shown in (A) and (C). (B) and (D) Cilia lengths were quantified as described in Methods and plotted in order of increasing length. Mean cilia length was approximately 6.5 μm and 7.9 μm in control and *OCRL* siRNA treated cells respectively, and 4.7 μm, 4.5 μm, 3.9 μm, and 5.1 μm in Control cl.1, Control cl.2, KO cl.1, and KO cl.2 cells, respectively. Cilia lengths were measured for 67-88 cells per condition in two independent experiments using CRISPR/Cas9 clones and 95 cells per condition in one experiment using siRNA treated cells. Scale bars (A and C): 10 μm.

Video S1. Cell division in CRISPR/Cas9 control clone 1. Control cl.1 cells, plated sparsely, were stained with Draq5 and imaged every 15 min using a combination of confocal and transmitted light to visualize DNA content and cell morphology. At the beginning of imaging, one cell in the selected field (arrow) started in interphase and successfully divided into two cells (~120 min from the initiation of metaphase to completion of cytokinesis).

Video S2. Cell division in CRISPR/Cas9 KO clone 2 that resolves into two cells. *OCRL* KO cl.2 cells, plated sparsely, were stained with Draq5 and imaged every 15 min using a combination of confocal and transmitted light to visualize DNA content and cell morphology. One cell in the selected field (arrow) was followed throughout cell division. This cell successfully divides into two cells. The period from initiation of metaphase to completion of cytokinesis was ~180 min.

Video S3. Cell division in CRISPR/Cas9 KO clone 2 that resolves into one multinucleated cell. *OCRL* KO cl.2 cells, plated sparsely, were stained with Draq5 and imaged every 15 min using a combination of confocal and transmitted light to visualize DNA content and cell morphology. One cell in the selected field (arrow) was followed throughout cell division. This cell does not properly complete cell division as the cytokinetic bridge is never cleaved. Eventually, abscission is aborted and the cell resolves into a single multinucleated cell. The period from metaphase to aborted cell division is ~300 min, and is longer than the average division time for *OCRL* KO cells that successfully divided into two daughter cells.

Gliozzi et al.
Fig. S1

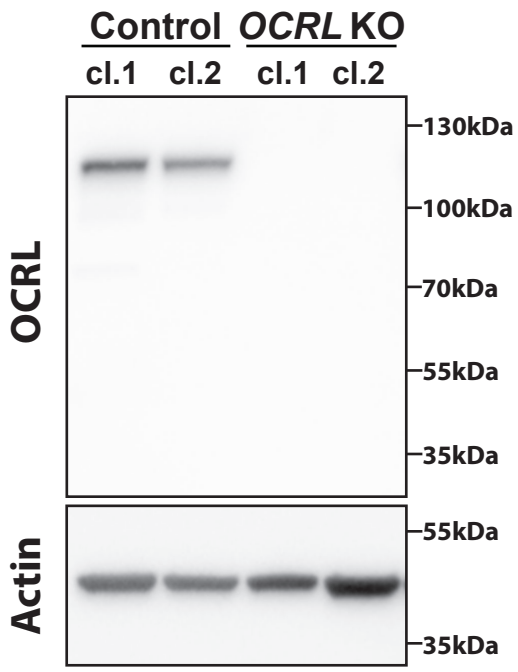

Gliozzi et al.
Fig. S2

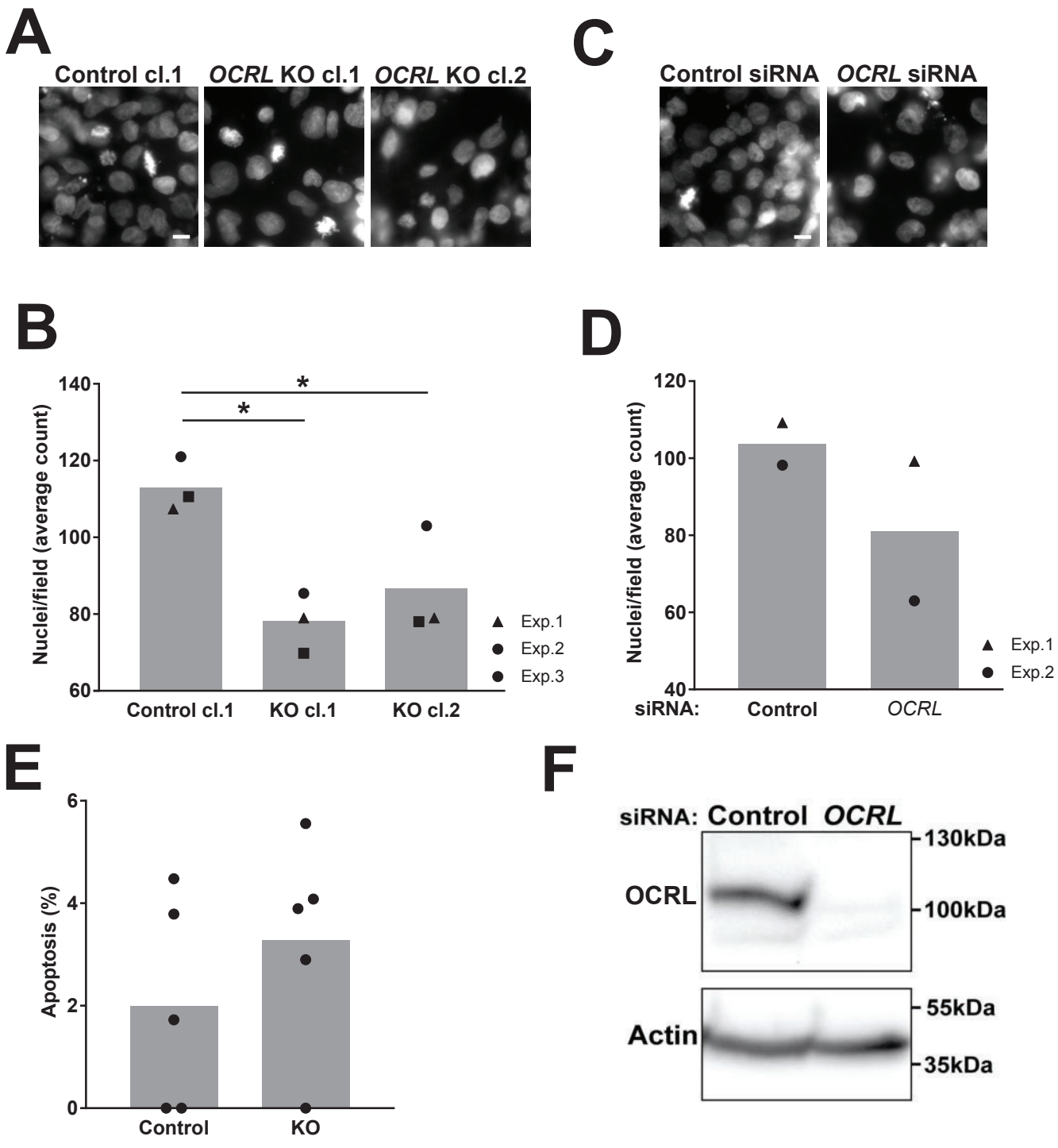

Gliozzi et al.
Fig. S3

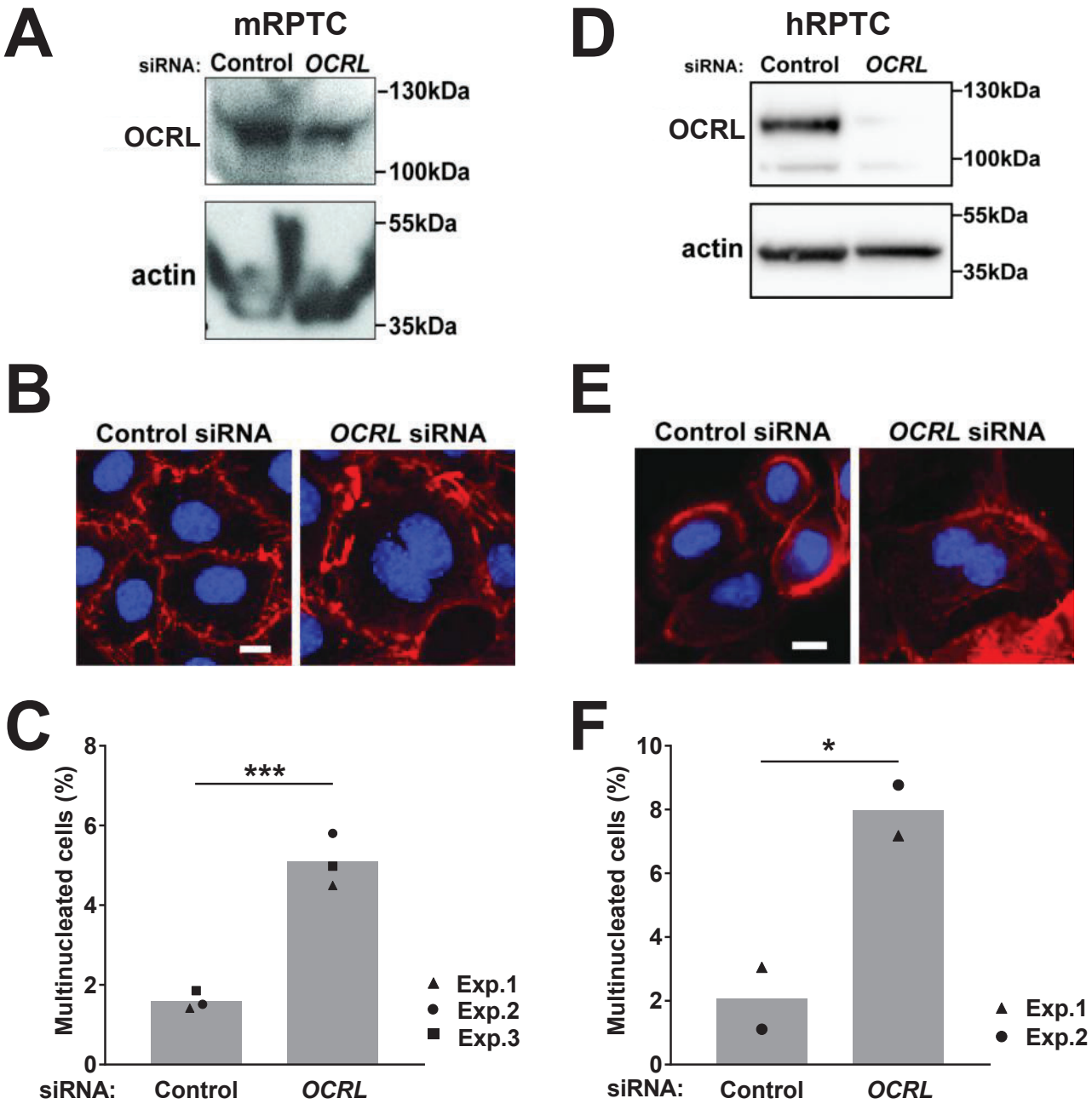

Gliozzi et al.
Fig. S4

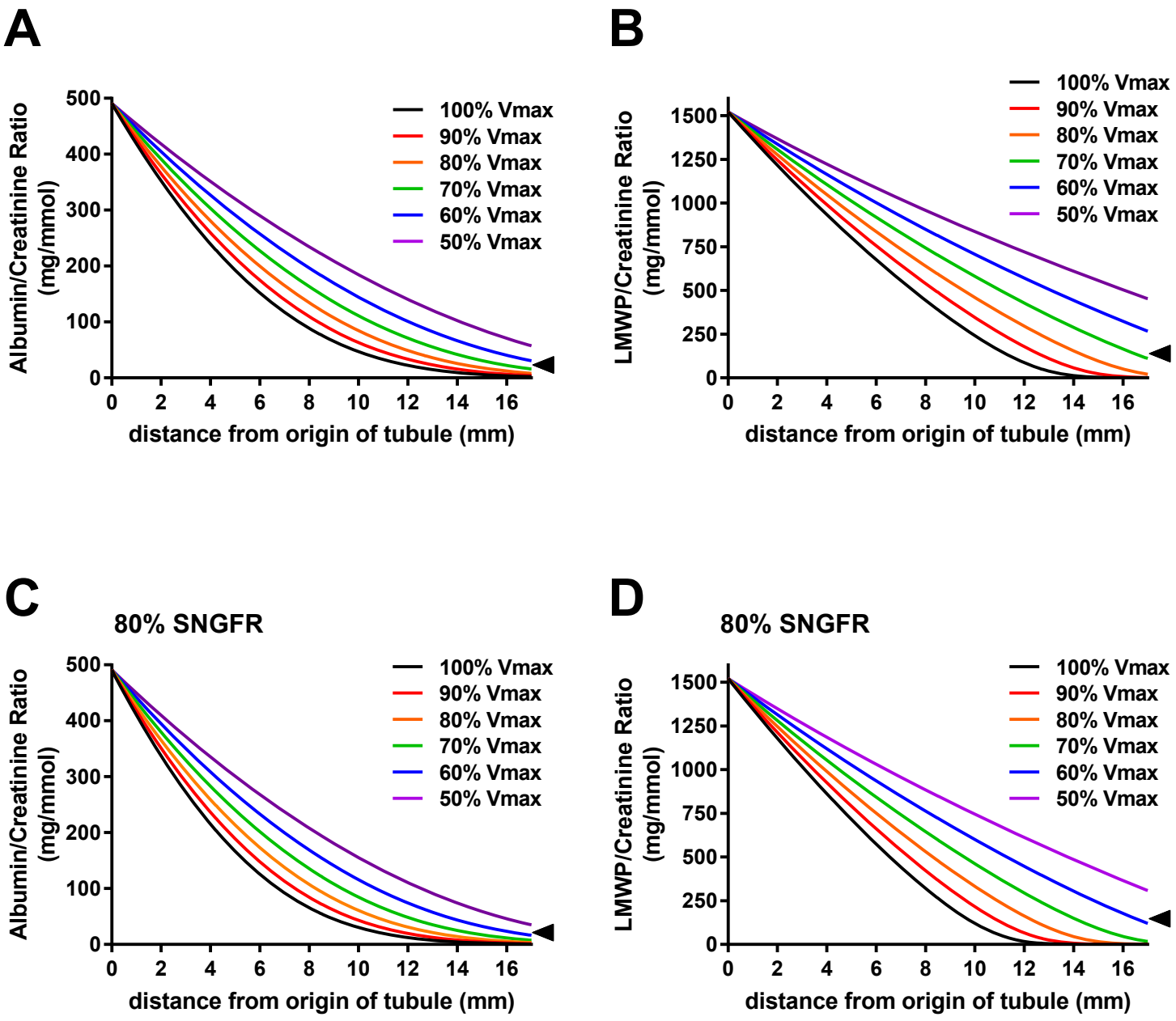

Gliozzi et al.
Fig. S5

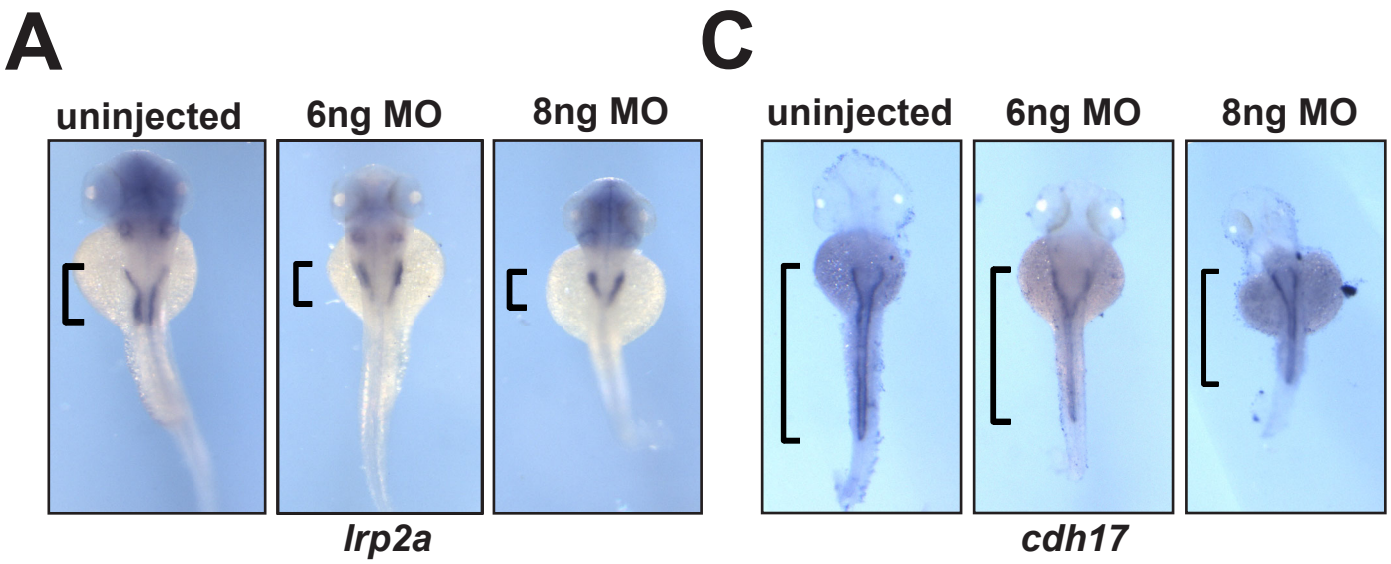

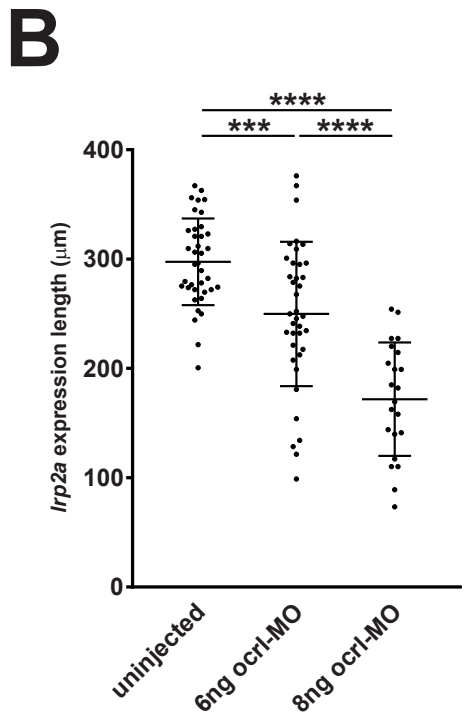

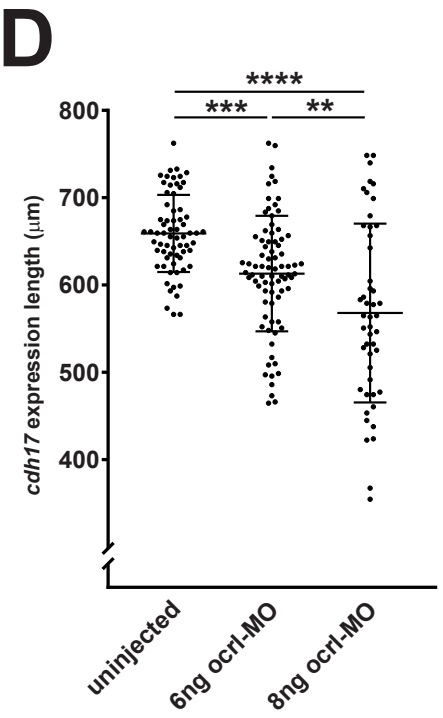

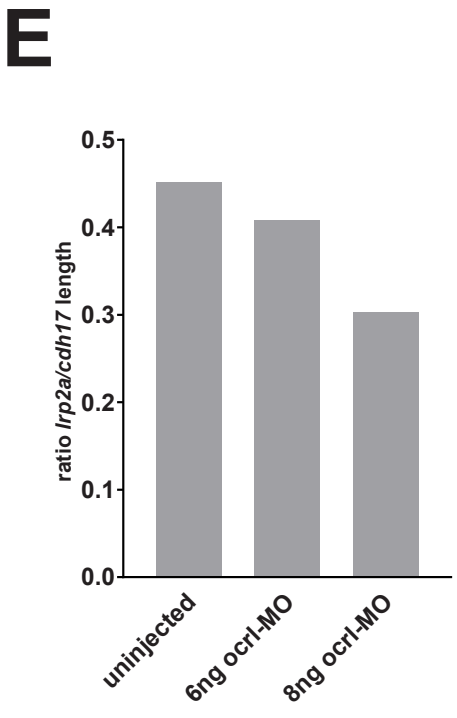

Gliozzi et al.
Fig. S6

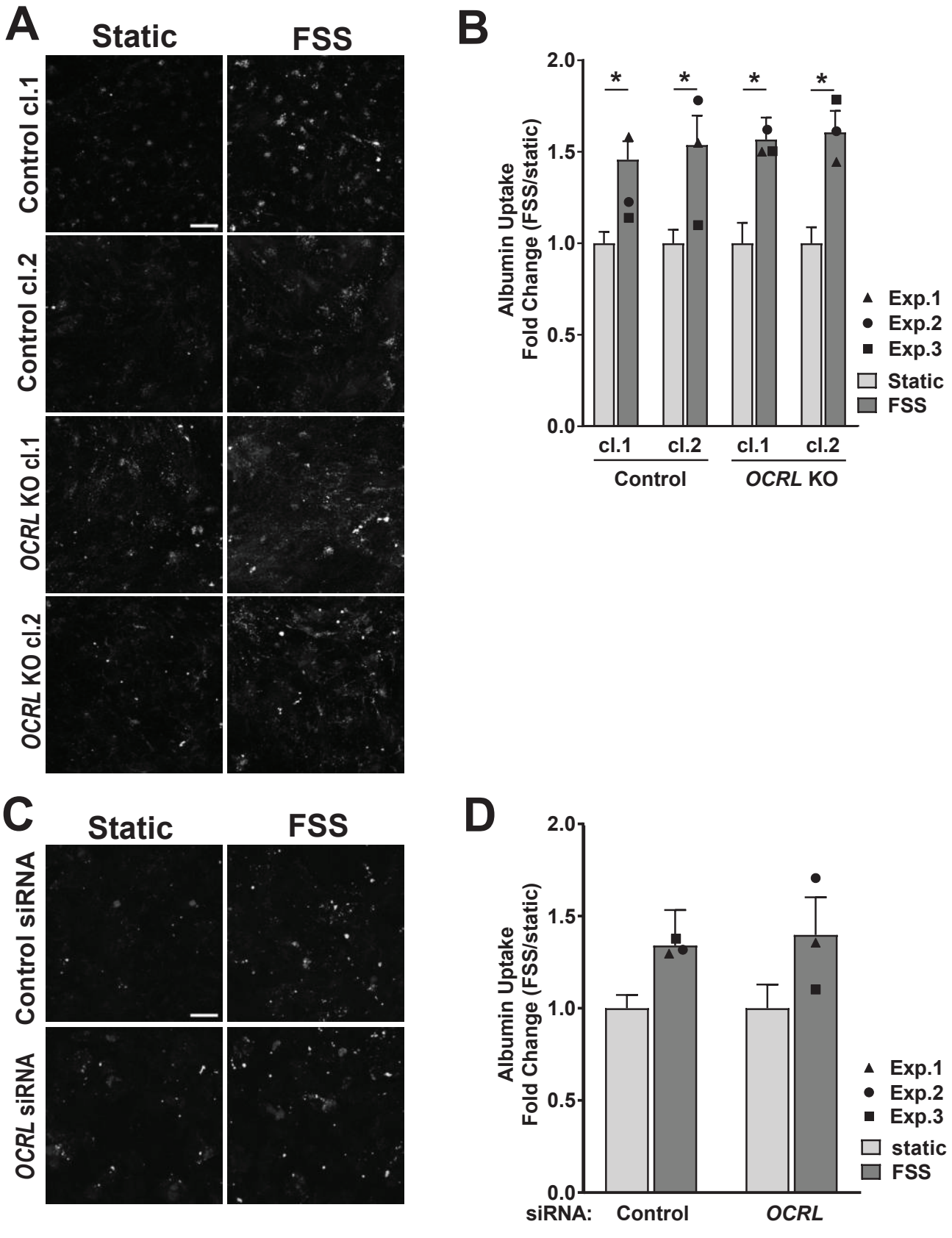

Gliozzi et al.
Fig. S7